



Heavy Flavor Production at the Tevatron

Chunhui Chen

(Representing the CDF and DØ Collaboration)

Department of Physics and Astronomy, University of Pennsylvania, Philadelphia, PA 19104, U.S.A.

Abstract. Using a subset of the current Run II data, the CDF and DØ have performed several measurements on heavy flavor production. In this paper, we present a new measurement of prompt charm meson production by CDF. We also report the latest CDF II measurements of inclusive J/Ψ production and b -production without requirement of minimum transverse momentum on J/Ψ and b -quark. They are the first measurements of the total inclusive J/Ψ and b quark cross section in the central rapidity region at a hadron collider. The results of J/Ψ cross section as a function of rapidity, and b -jet production cross section measured by DØ are also reviewed.

INTRODUCTION

Measurements of the production cross section of heavy flavor quarks (c and b quarks) in the $p\bar{p}$ collisions provide us an opportunity to test the prediction based on the Quantum Chromodynamics (QCD). Not only is QCD one of the four fundamental forces of the nature, but also many searches of new physics beyond Standard Model require a good understanding of the QCD background.

The Bottom quark production cross section has been measured by both the CDF and DØ experiments [1, 2] at the Fermilab Tevatron in $p\bar{p}$ collision at $\sqrt{s} = 1.8\text{TeV}$, and found to be about three times larger than the next-to-leading order (NLO) QCD calculation [3, 4]. Since then, several theoretical explanation has been proposed to solve the disagreement, such as the large contributions from the NNLO QCD processes, possible contribution from “new physics” [5] etc. Recently, a more accurate description of b quark fragmentation has reduced the discrepancy to a factor 1.7 [6]. Nevertheless, further experimental measurements on the heavy flavor production are essential to shed light on the remaining clouds of this long standing issue.

Since the end of Run I (1996), the Tevatron had undergone major upgrade. The center of mass energy in the $p\bar{p}$ collision was increased from $\sqrt{s} = 1.8\text{TeV}$ to $\sqrt{s} = 1.96\text{TeV}$. The large luminosity enhancement dramatically increases the discovery reach and moves the experimental program into a regime of precision hadron collider physics. At the same time, both CDF [7] and DØ [8] experimental collaborations significantly upgraded their detectors to enrich the physics capabilities, especially for the heavy flavor physics program. The Tevatron Run II data taking period started in April 2002, so far the ac-

celerator has delivered about 300pb^{-1} integrated luminosities, both experiments collected more than 200pb^{-1} physics quality data. In this paper, we will give a brief summary of the latest results on heavy flavor production from Tevatron Run II.

PROMPT CHARM MESON PRODUCTION CROSS SECTION

In order to help understanding the discrepancy between measured Run I Bottom quark cross section measurement and theoretical calculation, one can repeat previous measurement with better control of experimental uncertainties. An alternative approach is to examine the production rate of another heavy quark. Charm meson production cross sections have not been measured in $p\bar{p}$ collisions and may help to solve this disagreement. For CDF II upgrade, one of the crucial improvement with respect to the CDF I is the implementation of a Silicon Vertex Trigger (SVT) [9], which allows us to trigger on displaced tracks decayed from long-lived charm and bottom hadrons. With this trigger, large amount of fully reconstructed charm meson has been collected, opening a new window for heavy flavor production studies at hadron collider.

Using just $5.8 \pm 0.3\text{pb}^{-1}$ data, CDF performs a measurement of prompt charm meson production cross section [10]. The charm mesons are reconstructed in the following decay modes: $D^0 \rightarrow K^-\pi^+$, $D^{*+} \rightarrow D^0\pi^+$ with $D^0 \rightarrow K^-\pi^+$, $D^+ \rightarrow K^-\pi^+\pi^+$, $D_s^+ \rightarrow \phi\pi^+$ with $\phi \rightarrow K^+K^-$, and their charge conjugate, as shown in Fig. 1. We separate charm directly produced in $p\bar{p}$ interaction (prompt charm) from charm decayed from B

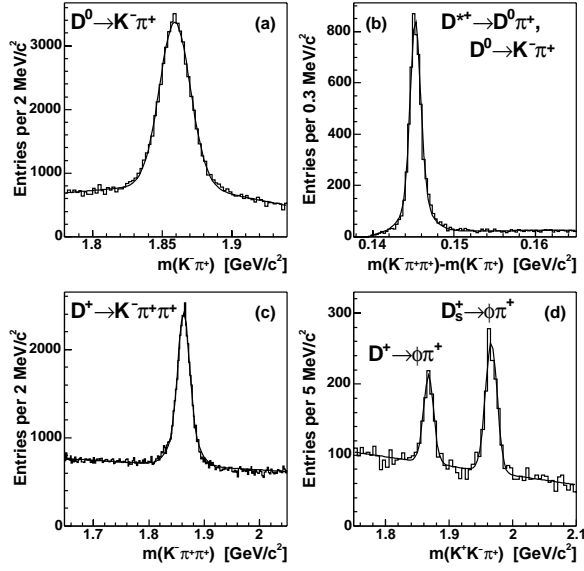


FIGURE 1. Charm signals summed over all p_T bins: (a) invariant mass distribution of $D^0 \rightarrow K^- \pi^+$ candidates; (b) mass difference distribution of $D^{*+} \rightarrow D^0 \pi^+$ candidates; (c) invariant mass distribution of $D^+ \rightarrow K^- \pi^+ \pi^+$ candidates; (d) invariant mass distribution of $D^+ \rightarrow \phi \pi^+$ and $D_s^+ \rightarrow \phi \pi^+$ candidates.

mesons (secondary charm) using the impact parameter of the charm candidate with respect to the primary interaction point. Prompt charm meson points to the beamline and its impact parameter is zero. The secondary charm meson candidate does not necessarily point back to the primary vertex, it has a rather wide impact parameter distribution. The shape of the impact parameter distribution of secondary charm is obtained from a Monte Carlo simulation. The detector impact parameter resolution is modeled from a sample of $K_S^0 \rightarrow \pi^+ \pi^-$ decays that satisfy the same trigger requirement. The prompt charm fraction is measured as a function of charm meson p_T . Average over all p_T bins, $(86.6 \pm 0.4)\%$ of the D^0 mesons, $(88.1 \pm 1.1)\%$ of D^{*+} , $(89.1 \pm 0.4)\%$ of D^+ , and $(77.3 \pm 3.8)\%$ of D_s^+ are promptly produced (statistical uncertainties only).

The measured prompt charm meson integrated cross section are found to be $\sigma(D^0, p_T \geq 5.5 \text{ GeV}/c, |y| \leq 1) = 13.3 \pm 0.2 \pm 1.5 \mu\text{b}$, $\sigma(D^{*+}, p_T \geq 6.0 \text{ GeV}/c, |y| \leq 1) = 5.2 \pm 0.1 \pm 0.8 \mu\text{b}$, $\sigma(D^+, p_T \geq 6.0 \text{ GeV}/c, |y| \leq 1) = 4.3 \pm 0.1 \pm 0.7 \mu\text{b}$ and $\sigma(D_s^+, p_T \geq 8.0 \text{ GeV}/c, |y| \leq 1) = 0.75 \pm 0.05 \pm 0.22 \mu\text{b}$, where the first uncertainty is statistical and the second systematic. The measured differential cross sections are compared to two recent calculations [11, 12], as shown in Fig. 2 and Fig. 3. They are higher than the theoretical predictions by about 100% at low p_T and 50% at high p_T . However, they are compatible within uncertainties. The same models also

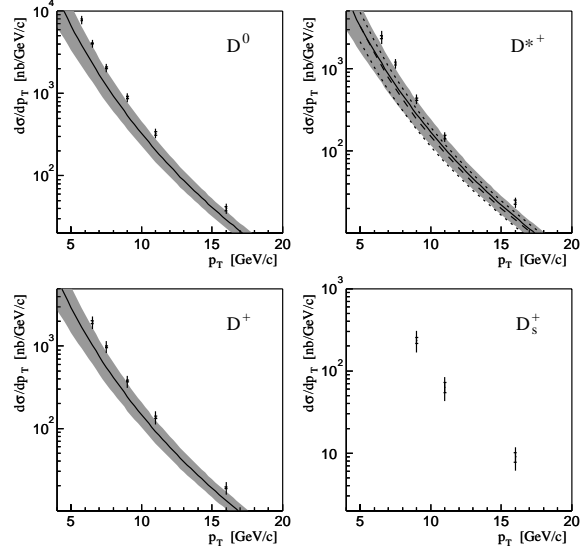


FIGURE 2. The measured differential cross section measurements for $|y| \leq 1$, shown by the points. The inner bars represent the statistical uncertainties; the outer bars are the quadratic sums of the statistical and systematic uncertainties. The solid curves are the theoretical predictions from Cacciari and Nason [11], with the uncertainties indicated by the shaded bands. The dashed curve shown with the D^{*+} cross section is the theoretical prediction from Kniehl [12]; the dotted lines indicate the uncertainty. No prediction is available yet for D_s^+ production.

underestimate B meson production at $\sqrt{s} = 1.8 \text{ TeV}$ by similar factors [2, 6, 13].

INCLUSIVE J/Ψ PRODUCTION CROSS SECTION

The CDF II detector has improved the dimuon trigger system with a lower threshold of $1.5 \text{ GeV}/c$. This allows us to trigger the $J/\Psi \rightarrow \mu^- \mu^+$ event with transverse momentum all the way down to $p_T(J/\Psi) = 0 \text{ GeV}/c$. Using about 39.7 pb^{-1} data, CDF reconstructed 299800 ± 800 J/Ψ candidates (statistical uncertainty only), as shown in Fig. 4. A new measurement of the total inclusive J/Ψ cross section in the central rapidity region $|y| \leq 0.6$ has been carried out. This is the first measurement of the total inclusive J/Ψ cross section in the central rapidity region at a hadron collider. The differential cross section is shown in Fig. 5, and the integrated cross section is measured to be:

$$\begin{aligned} \sigma(p\bar{p} \rightarrow J/\Psi X, |y(J/\Psi) \leq 0.6) \times Br(J/\Psi \rightarrow \mu\mu) \\ = 240 \pm 1(\text{stat})_{-28}^{+35}(\text{syst}) \text{ nb}, \end{aligned} \quad (1)$$

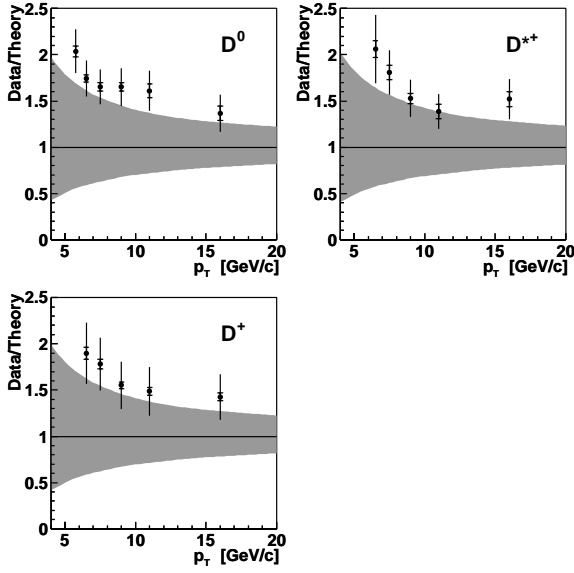


FIGURE 3. Ratio of the measured cross sections to the theoretical calculation from Cacciari and Nason. The inner error bar represents the statistical uncertainty, the outer error bar the quadratic sum of the statistical and systematic uncertainty. The hatched band represents the uncertainty from varying the renormalization and factorization scale.

Taking advantage of the large azimuth coverage of its muon system, the $D\bar{O}$ measured the differential cross section of the inclusive J/Ψ as a function of the rapidity using 4.74 pb^{-1} . The distribution is shown in Fig. 6.

BOTTOM QUARK PRODUCTION CROSS SECTION

The Run I central b -quark production cross section measured by CDF and $D\bar{O}$ has a minimum transverse momentum cut on the b -hadrons due to the trigger requirements. Since those measurements only explore a small fraction ($\sim 10\%$) of the b -hadron p_T spectrum, it is not clear from the data whether the excess over the theory is due to an overall discrepancy of the $b\bar{b}$ production rate, or it is caused by a shift in the spectrum toward higher p_T . An inclusive measurement of bottom quark production over all transverse momentum can certainly help resolve this ambiguity.

Notice that large fraction of b -hadron H_b decays to J/Ψ final states, where H_b denotes both hadron and anti-hadron. CDF performed an analysis to extract the inclusive b -hadron cross section from the measured inclusive J/Ψ production cross section. Due to the long live lifetime of the b -hadrons, the vertex of the J/Ψ decayed from a b -hadron (secondary J/Ψ) is usually hundreds microns away from the primary vertex, while for

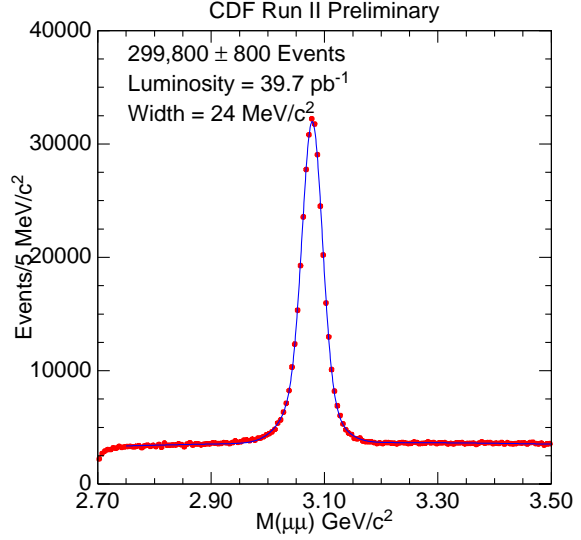


FIGURE 4. The invariant mass distribution of triggered J/Ψ events reconstructed in the 39.7 pb^{-1} of CDF II data.

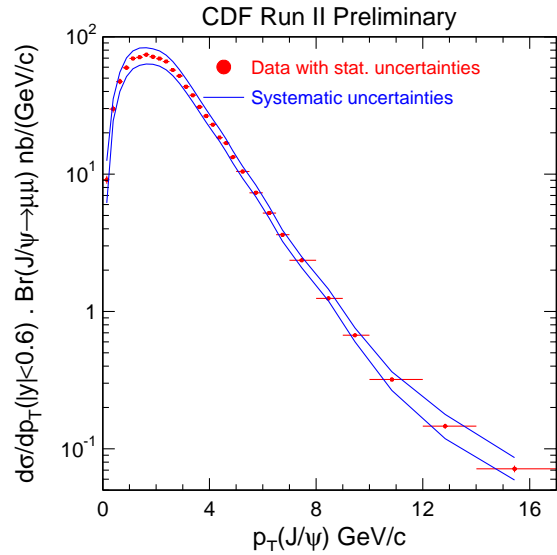


FIGURE 5. The differential cross section for inclusive J/Ψ as a function of p_T with $|y| \leq 0.6$.

the prompt J/Ψ 's, which are directly produced or decayed from higher charmonium states, their vertex are at the proton-antiproton interaction point. As the result, we can statistically separate these two components by examining the projected J/Ψ decay distance along its

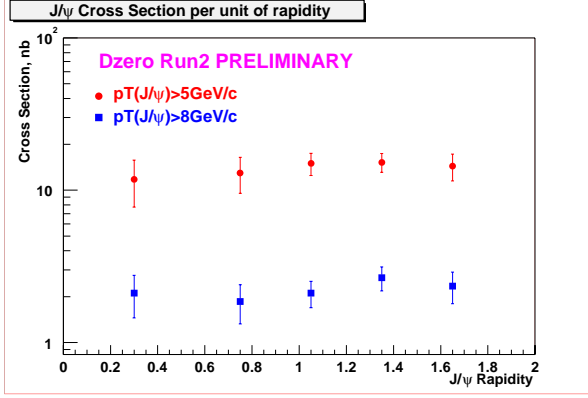


FIGURE 6. The differential cross section for J/Ψ as a function of $|y|$.

transverse momentum. The measured b -fraction is then applied to the previously measured inclusive J/Ψ cross section to obtain the differential production cross section of $H_b \rightarrow J/\Psi X$ as a function of $p_T(J/\Psi)$. However, the above algorithm to extract b -fraction does not work for J/Ψ candidate with low transverse momentum, because a b -hadron with low p_T does not travel far away from the primary vertex in the transverse plane. Therefore a minimum $p_T(J/\Psi) \geq 1.25 \text{ GeV}/c$ requirement is imposed for the b -hadron cross section measurement as a function of $p_T(J/\Psi)$ in order to have a reliable determination of b -fraction. The measured differential cross section result is shown in Fig. 7.

Luckily, the b -hadron decayed at rest can still transfer a few (~ 1.7) GeV/c transverse momentum to its J/Ψ daughter because of the large b -hadron mass. The knowledge of the secondary J/Ψ production with transverse momenta less than $2.0 \text{ GeV}/c$ allows us to probe the b -hadrons with low transverse momenta down to zero. Therefore using the measured b -hadron differential cross section with $1.25 \leq p_T(J/\Psi) \leq 17.0 \text{ GeV}/c$, we are able to extract the b -hadron differential cross section as a function of $p_T(H_b)$ down to $p_T(H_b) = 0 \text{ GeV}/c$. To do so, we perform a convolution that is based on the Monte Carlo template of the b -hadron transverse momentum distribution. The unfolding procedure is then repeated using the measured b -hadron production spectrum as the input spectrum for the next iteration, until the χ^2 comparison between the input and output spectrum calculated after each iteration becomes stable. The measured b -hadron cross section as a function of $p_T(H_b)$ is plotted in Fig. 8. The total b -hadron cross section is found to be

$$\begin{aligned} & \sigma(p\bar{p} \rightarrow H_b X, |y(H_b)| \leq 0.6) \times Br(H_b \rightarrow J/\Psi X) \\ & \times Br(J/\Psi \rightarrow \mu\mu) = 24.5 \pm 0.5(stat)_{-3.9}^{+4.7}(syst) \text{ nb}, \end{aligned} \quad (2)$$

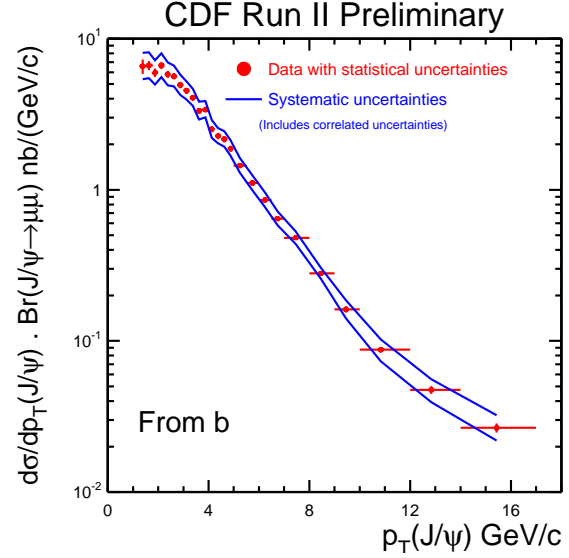


FIGURE 7. b -hadron differential cross section as a function of $p_T(J/\Psi)$.

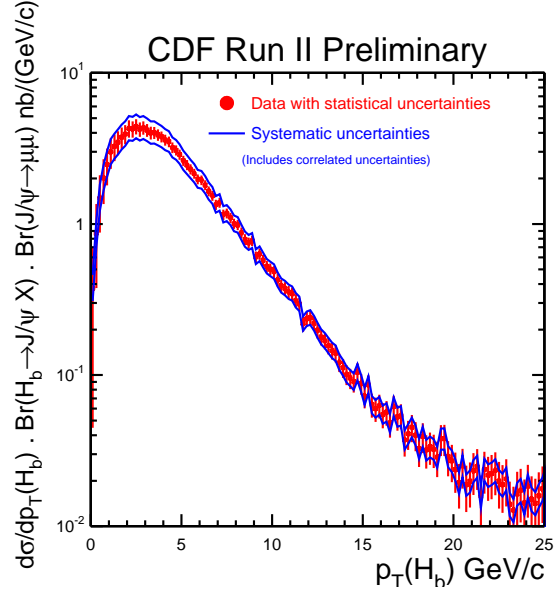


FIGURE 8. b -hadron differential cross section as a function of $p_T(H_b)$ with $|y| \leq 0.6$.

The total single b -quark cross section is obtained by divided this measurement by two, the branching fractions, and the rapidity correction factors obtained from MC. We

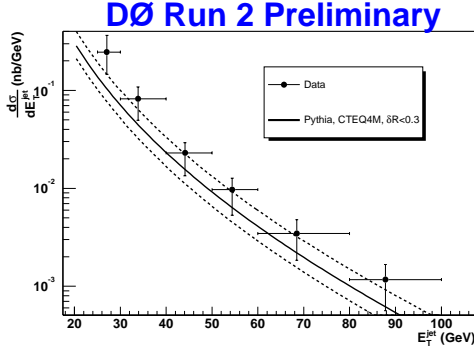


FIGURE 9. Measured Run II b -jet cross section compared to theoretical prediction.

find:

$$\sigma(p\bar{p} \rightarrow \bar{b}X, |y(b)| \leq 0.6) \quad (3)$$

$$= 18.0 \pm 0.4(stat) \pm 3.8(syst) \mu\text{b},$$

and

$$\sigma(p\bar{p} \rightarrow \bar{b}X, |y(b)| \leq 1) \quad (4)$$

$$= 29.4 \pm 0.6(stat) \pm 6.2(syst) \mu\text{b}.$$

B-JET PRODUCTION CROSS SECTION

Using 3.4pb^{-1} of data, a b -jet production cross section analysis has been performed by DØ. The candidate event is selected by associating a muon track with a jet, which is defined with $R = \sqrt{\Delta\eta^2 + \Delta\phi^2}$ cone algorithm. Notice the fact that the muon decayed from b quark has a higher transverse momentum with respect to the net momentum vector of combined muon and jet, the corresponding distribution is then used to fit the b -jet fraction. The signal template is modeled from a $b \rightarrow \mu$ Monte Carlo simulation, and the background template is extracted from 1.5 million QCD events. After correcting the muon and jet reconstruction efficiency, and the calorimeter jet energy resolution, the b -jet cross section is obtained. The preliminary result is shown in Fig. 9 compared to the theoretical prediction. This measurement is consistent with the previous Run I measurement [14].

CONCLUSION

The understanding of the heavy flavor production is currently one of the most important challenges faced by QCD. In this paper, we present the most recent measurements from CDF and DØ experiments. Given large amount of data that have already been collected, rapid improvement of Tevatron performance, and further understanding of the detector, we expect that much more

precise measurements on the heavy flavor production will be available in the near future. At the same time, several other analyses have also been carried out to explore other aspects of heavy flavor production mechanism, such as the $b\bar{b}$ correlation and $c\bar{c}$ correlation during the production. In the next a few years, a combination of better experimental data and improved theory should advance our knowledges of the heavy quarks production.

ACKNOWLEDGMENTS

We thank the CDF and DØ collaboration for their helps while preparing this paper. We also thank the conference organizers for a wonderful meeting.

REFERENCES

1. Abbott, B., et al., *Phys. Lett.*, **B487**, 264–272 (2000).
2. Acosta, D., et al., *Phys. Rev.*, **D65**, 052005 (2002).
3. Nason, P., Dawson, S., and Ellis, R. K., *Nucl. Phys.*, **B327**, 49–92 (1989).
4. Albajar, C., et al., *Phys. Lett.*, **B186**, 237 (1987).
5. Berger, E. L., et al., *Phys. Rev. Lett.*, **86**, 4231–4234 (2001).
6. Cacciari, M., and Nason, P., *Phys. Rev. Lett.*, **89**, 122003 (2002).
7. Blair, R., et al. (1996), FERMILAB-PUB-96-390-E.
8. Abachi, S. (1996), FERMILAB-PUB-96-357-E.
9. Ashmanskas, W., et al., *Nucl. Instrum. Meth.*, **A447**, 218–222 (2000).
10. Acosta, D., et al., *Phys. Rev. Lett.*, **91**, 241804 (2003).
11. Cacciari, M., and Nason, P., *JHEP*, **09**, 006 (2003).
12. Kniehl, B. (Private communication), Their calculation employs the method described in B.A. Kniehl, G. Kramer, B. Potter, *Nucl. Phys.* **B597**, 337–369 (2001).
13. Binnewies, J., Kniehl, B. A., and Kramer, G., *Phys. Rev.*, **D58**, 034016 (1998).
14. Abbott, B., et al., *Phys. Rev. Lett.*, **85**, 5068–5073 (2000).